Observations of the turbulence in the scrape-off-layer of Alcator C-Mod and comparisons with simulation[a)]

J. L. Terry[b)]
MIT Plasma Science and Fusion Center, Cambridge, Massachusetts 02139

S. J. Zweben
Princeton Plasma Physics Laboratory, Princeton, New Jersey 08543

K. Hallatschek
Max Planck Institute of Plasma Physics, Garching, Germany

B. LaBombard
MIT Plasma Science and Fusion Center, Cambridge, Massachusetts 02139

R. J. Maqueda
Los Alamos National Laboratories, Los Alamos, New Mexico 87545

B. Bai, C. J. Boswell, M. Greenwald, and D. Kopon
MIT Plasma Science and Fusion Center, Cambridge, Massachusetts 02139

W. M. Nevins
Lawrence Livermore Laboratory, Livermore, California 94550

C. S. Pitcher
MIT Plasma Science and Fusion Center, Cambridge, Massachusetts 02139

B. N. Rogers
Dartmouth University, Hanover, New Hampshire 03755

D. P. Stotler
Princeton Plasma Physics Laboratory, Princeton, New Jersey 08543

X. Q. Xu
Lawrence Livermore Laboratory, Livermore, California 94550

(Received 11 November 2002; accepted 4 February 2003)

The intermittent turbulent transport in the scrape-off-layer (SOL) of Alcator C-Mod [I.H. Hutchinson, R. Boivin, P.T. Bonoli *et al.*, Nucl. Fusion **41**, 1391 (2001)] is studied experimentally by imaging with a very high density of spatial measurements. The two-dimensional structure and dynamics of emission from a localized gas puff are observed, and intermittent features (also sometimes called ''filaments'' or ''blobs'') are typically seen. The characteristics of the spatial structure of the turbulence and their relationship to the time-averaged SOL profiles are discussed and compared with those measured on the National Spherical Torus Experiment [M. Ono, S. M. Kaye, Y.-K. M. Pong *et al.*, Nucl. Fusion **40**, 557 (2000)]. The experimental observations are compared also with three-dimensional nonlinear numerical simulations of edge turbulence. Radial profiles of the poloidal wave number spectra and the poloidal scale length from the simulations are in reasonable agreement with those obtained from the experimental images, once the response of the optical system is accounted for. The resistive ballooning mode is the dominant linear instability in the simulations. The ballooning character of the turbulence is also consistent with fluctuation measurements made at the inboard and outboard midplane, where normalized fluctuation levels are found to be about 10 times smaller on the inboard side. For discharges near the density limit, turbulent structures are seen on closed flux surfaces. © *2003 American Institute of Physics*. [DOI: 10.1063/1.1564090]

I. INTRODUCTON

Evidence for intermittent convective radial transport in the outboard scrape-off-layers (SOL) of tokamaks has existed for a number of years.[1–4] Recently, studies aimed at investigating this phenomenon have yielded a much clearer picture of the SOL transport and its implications on main chamber recycling,[5,6] divertor operation, and possibly density limits.[7,8] Typically, detailed measurements of the turbulence have come from single point or multipoint probe or optical measurements in the outboard SOL, and they generally show very strong evidence for intermittent, convective particle transport there, leading to the nearly flat temperature and density profiles observed in the far-SOL of many devices. The statistics of the fluctuations are strongly non-

[a)]Paper KI2 1, Bull. Am. Phys. Soc. **47**, 182 (2002).
[b)]Invited speaker.

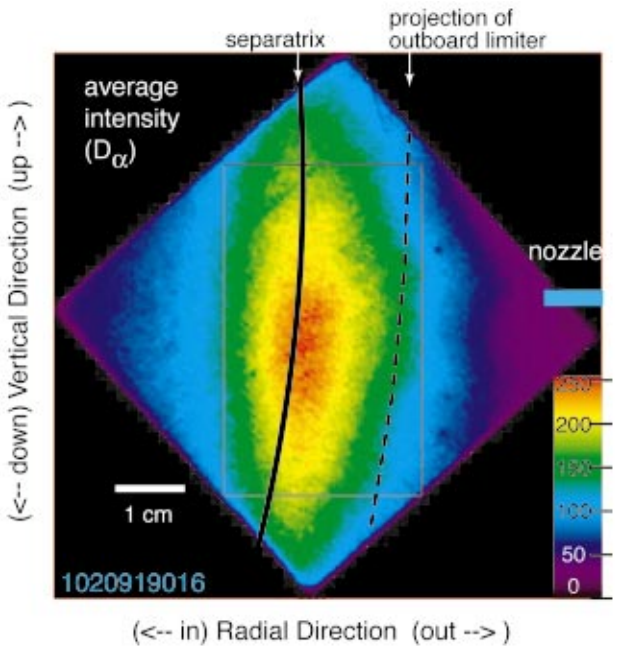

FIG. 1. (Color) The time-averaged image of D_α brightness from the gas puff on the outboard midplane. The X-section is the plane perpendicular to the local field. Also shown are the separatrix, the projection of the outboard limiter, and the rectangular box inside of which the k_{pol} spectra and L_{pol} are calculated. The poloidal variation in the average image is due to the poloidal distribution of the gas puffed from the nozzle, whose location is also shown.

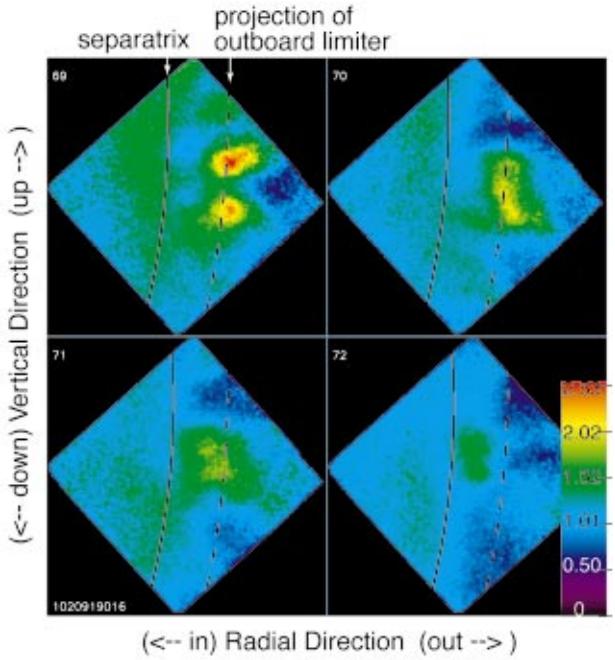

FIG. 2. (Color) Four consecutive ''normalized'' images calculated by dividing each 2 μs snapshot by the time-averaged image. Two large-amplitude fluctuations—blobs—are seen in the first image. Each of the other three images shows smaller amplitude structures existing primarily outside the separatrix, as well as emission ''holes,'' where the snapshot emission is less than the average. The scale shows the emission relative to the average.

Gaussian,[9,10] with positive skewness and kurtosis, and the large amplitude events can be responsible for large fractions of the cross-field particle and heat transport.[10] Understanding the physical causes and mechanisms of this intermittent transport is important since it can dominate the scrape-off-layer transport.[6,10,11] Indeed there appears to be a ''universality'' [12] to the intermittency that extends to stellarators[13] and even linear devices. The two magnetic confinement devices reported on here, Alcator C-Mod and National Spherical Torus Experiment (NSTX) as well as other tokamaks,[14–16] exhibit many qualitatively similar features, e.g., large, intermittent events, high levels of SOL turbulence, non-Gaussian turbulence statistics, and poloidal and radial motion of localized features. Yet the SOL plasmas in these devices are different in many respects, e.g., B_T, $\lambda_{\mathrm{ei}}/L_c$, ρ_s, gradient scale length. It is the purpose of this paper to report the experimental observations from C-Mod and to compare the experimental results with those of NSTX and with three-dimensional (3D) nonlinear simulations of the edge plasma in hopes of understanding the physical mechanisms responsible for the observed turbulence.

II. EXPERIMENTAL IMAGING OF TURBULENCE

Although some investigations of the extended spatial structure of edge turbulence have been carried out,[17–19] including direct imaging of the density fluctuations using beam emission spectroscopy (BES),[15,16,20] the majority of investigations of edge turbulence have utilized localized probes, and much of the present understanding of the turbulent transport and statistics come from probe measurements and analyses. A new technique designed to study the detailed spatial structure of the turbulence has recently been developed,[21–23] yielding additional information that can be directly compared with edge-turbulence modeling. In Alcator C-Mod and in NSTX the edge/SOL turbulence is imaged vs time with a very high density of high-resolution spatial measurements,[22–24] in addition to being studied with probes. This paper will give the experimental details and results from Alcator C-Mod and a comparison with NSTX results. The detailed NSTX results will be given in a subsequent paper.

The imaging is accomplished by viewing (parallel to the local field) line emission from a localized gas puff. Since the turbulence is known to have relatively long parallel wavelengths and to be closely aligned with the field, the gas puff provides spatial localization of emission in the parallel dimension and allows high resolution images in the dimensions perpendicular to the field. The detailed 2D structure and dynamics of the emission are then measured using gated (0.5 to 10 μs) and high frame-rate (up to 1 MHz) cameras, filtered for line emission from the puffed gas (D_2 or He). More details and a schematic of the setup on C-Mod are given in Ref. 22. The NSTX system is discussed in Ref. 23.

An example of a *time-averaged* emission pattern is shown in Fig. 1. The field-of-view is shown as the $\sim 6 \times 6$ cm diamond shaped region and is centered near the typical separatrix location at the outboard side of the tokamak, 2.5 cm below the midplane. Regions both inside and outside the separatrix and in the shadow of outboard limiters are viewed. The atomic physics ''windows'' the average emission region, limited on the hot side by ionization and on the wall side by lack of excitation. However, individual images

TABLE I. Comparison of quantities characterizing SOLs of specific L-mode plasmas, evaluated at the outboard midplane. In the C-Mod cases the evaluations are made at $\rho=6$ mm; in NSTX at $\rho\sim1$ density e-folding length outside the separatrix.

	C-Mod "high" field (No. 1020919006)	C-Mod "low" field (No. 1020919016)	NSTX (No. 109033)
B_T^{SOL}	4.5 T	2.1 T	0.25 T
I_p	1.0 MA	0.45 MA	0.9 MA
n_e	1.4×10^{19} m^{-3}	2.2×10^{19} m^{-3}	6×10^{18} m^{-3}
T_e	23 eV	22 eV	13 eV
L_p^{perp}	4 mm	5 mm	30 mm
ρ_S	0.15 mm	0.32 mm	2 mm
L_c	5 m	5 m	5 m
$L_0^{\mathrm{resist\ ball}}$	$\sim$3 mm	$\sim$7 mm	$\sim$10 mm
$L_{\mathrm{pol}}^{\mathrm{turb}}$	$\sim$7 mm	$\sim$10 mm	$\sim$40 mm
$\tau_{\mathrm{auto\ corr}}$	~10 μs	~10 μs	~40 μs
$I_{\mathrm{sat}}^{\mathrm{RMS}}/I_{\mathrm{sat}}$	$\sim$40%	$\sim$40%	$\sim$40%
λ_{ei}/L_c	0.09	0.06	0.07
β	1×10^{-5}	9×10^{-5}	10^{-3}

vary significantly from the average, and complex emission patterns are typically observed. Some of the snapshots and movies show isolated regions of strong emission. These are almost certainly the large amplitude ion-saturation-current and floating-potential events seen on probes. They have been called striations, filaments, blobs, intermittent plasma objects (IPOs), and avaloids by different investigators and, as mentioned above, have been shown to be responsible for large fractions of the perpendicular particle and heat transport. The blob designation comes from the appearance of the perturbation when viewed in the cross section, along the magnetic field. It is important to keep in mind that these fluctuations have relatively long, but finite (see Sec. V) parallel wavelengths.[1] Although the blobs are evident in the raw images, they are even clearer in images made by dividing out the average emission pattern. Four such "normalized" snapshots taken 17 ms apart are shown in Fig. 2. (The turbulence is completely uncorrelated between these snapshots.) Two blobs are clearly seen in the first frame. The other three frames show features, including "holes," mostly outside the separatrix and with significantly smaller amplitudes. Note that the scale shows the emission relative to the average, i.e., a color value of 2 is twice the time-averaged image emission. "Wave-like" poloidal structures are also sometimes observed.

Obviously, when using this "gas-puff-imaging" technique, the images are of line emission, not of quantities of more direct interest, like density and temperature. The atomic physics that converts the density and temperature fluctuations into fluctuations in emission complicate the quantitative interpretation.[22,25] Nonetheless, the emission fluctuations are the result of fluctuations in the "background" plasma, and *not* properties of the gas puff.[22] The details will not be repeated here except to say that within the "windowed" region set by the atomic physics, the emission responds promptly to the fluctuations approximately as $n_e^{\alpha}T_e^{\beta}$, with both α and β between 0.3 and 1.4.[25] In our quantitative comparisons with the numerical simulations

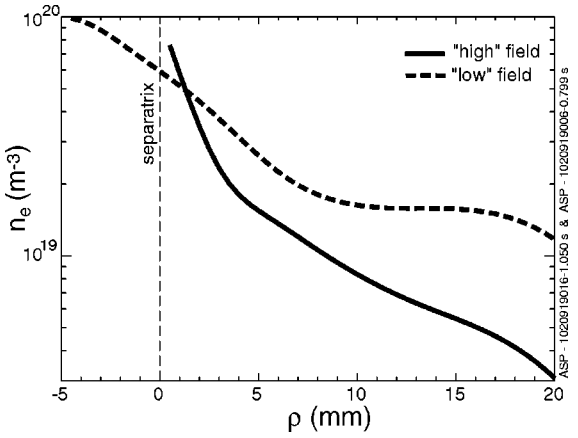

FIG. 3. SOL density profiles for the two cases discussed, as measured by an outboard reciprocating probe located $\sim$10 cm above the outside midplane.

(Sec. IV), we post-process the simulation n_e, T_e results to compute the emission, rather than trying to unfold the fluctuating temperature and density fields from the experimental images.

III. IMAGE ANALYSES

In order to analyze the images, the time-averaged emission is computed from a series of individual images (e.g., Fig. 1), and the individual frames are then normalized by that average image. This yields images showing the fractional changes from the time average (e.g., Fig. 2). The normalized images are then analyzed to produce wave number spectra of the normalized fluctuations in the poloidal and radial planes. In addition, the poloidal autocorrelation functions are calculated, and the poloidal autocorrelation lengths vs radius are calculated. The autocorrelation length serves as a simple measure of the size scale of the turbulence and is defined as that spatial translation for which the autocorrelation function decreases to 0.5. These analyses are done over the rectangular box shown in Fig. 1. No account is taken of the small poloidal curvature of the flux surfaces within this box, i.e., vertical is taken to be poloidal. This assumption has a negligible effect on the experimental poloidal structure sizes, at least for the structure sizes typical in the experiment, i.e., poloidal correlation lengths $\sim$10 mm and ratios of poloidal to radial correlation lengths <2.

We present here analyses of two discharges in C-Mod (see Table I), a "high" field case with $B_T=6.1$ T, $I_p=1.0$ MA and $n_e/n_{\mathrm{GW}}=0.2$, and a "low" field case with $B_T=2.85$ T, $I_p=0.45$ MA, and $n_e/n_{\mathrm{GW}}=0.45$. (n_{GW} is the Greenwald density, $I_p(\mathrm{MA})/[\pi a(m)^2]$ in units of 10^{20} m^{-3}, where a is the minor radius.) The two different field strengths mean that the ion gyroradii are different; ρ_S in the SOL is 0.15 and 0.32 mm, respectively. [$\rho_S=c_s/\Omega_{ci}$, where $c_s=(T_e/m_i)^{0.5}$, i.e., the ion gyroradius evaluated with the electron temperature.] These discharges have approximately the same edge safety factor and connection length. They were chosen to examine the scaling of the turbulence characteristics with field and ρ_S (a factor of 2.1) and with normalized density (a factor of 0.4). However, it is also worth noting that the collisionality, λ_{ei}/L_c, is 50% higher for the "high" field case. (λ_{ei} is the electron–ion mean free path; L_c

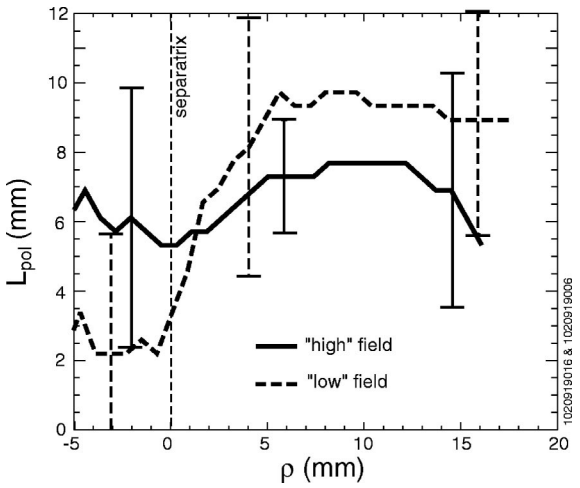

FIG. 4. Experimental L_{pol} vs ρ for the two cases discussed.

is the parallel connection length.) Comparison of discharges with differing *normalized* densities was chosen because of the possible link between edge turbulence and density limits.[7] Nonetheless, scaling with collisionality/density is also of interest, since transport in the near-SOL has been shown to depend on it.[26] The time-averaged SOL density profiles at the time of interest for these two shots are shown in Fig. 3. The profiles clearly have different SOL gradients and different far-SOL densities. The perpendicular particle fluxes are different as well (~two times higher in the "low" field, shallower gradient case). Shown in Fig. 4 are the respective poloidal correlation lengths (L_{pol}) vs ρ. [ρ is the distance outside the last closed flux surface (LCFS) mapped along flux surfaces to the outside midplane.] Outside $\rho \approx 3$ mm, the "low" field case has a somewhat higher correlation length (9–10 mm compared to 6–8 mm) although the difference is within the error bars for each measurement. (The error bars are ± 1 standard deviation of the statistical frame-to-frame variation.) Inside the separatrix L_{pol} is smaller in the "low" field case, again with some overlap of the error bars. Nonetheless, the trends and values of L_{pol} vs ρ found in these two discharges are reproducible in other discharges with similar parameters. For example, the "high" field case has little variation of L_{pol} with ρ and is similar in that respect to the C-Mod discharge analyzed in Ref. 22, which had similar plasma parameters. Nonetheless, the uncertainties are large enough that clearly significant differences in L_{pol} between the two cases are masked. A linear scaling with ρ_S is allowed, but is certainly not apparent.

In Figs. 5 and 6 are shown the k_{pol} spectra from the normalized images and the normalized levels of ion saturation current, I_{sat}^{RMS}/I_{sat} (from probes), both vs ρ. The amplitudes (color scale) of the k spectra for the "high" and "low" field cases are similar, indicating similar normalized levels of turbulence, and consistent with the outboard probe data of Fig. 6. Note, however, that because the density in the "low" field case is significantly larger outside of $\rho \approx 3$ mm, the absolute RMS fluctuation level is also larger. The falloff of Fourier amplitude, $A(k)$, with k outside of $\rho = 0$ is somewhat less steep in the "high" field case, consistent with the L_{pol} comparison, since L_{pol} is proportional to $1/\Delta k_{pol}^{HWHM}$. We note that for $\rho > 6$ mm in the high field case and over the entire profile in the low field case, amplitudes decrease monotonically with k_{pol} from the minimum measured k_{pol} of $\sim 1.3\ cm^{-1}$ ($k_{pol}^{min}\ \rho_S \sim 0.02-0.04$). This minimum is determined by the poloidal extent of the analyzed image. For $0 < \rho < 6$ mm in the high field case there is an amplitude maximum around $2\ cm^{-1}$ ($k_{pol}\ \rho_S \sim 0.03$). Measurements of edge turbulence on the outboard side of the TEXTOR tokamak[19] also showed monotonically decreasing spectral power from a minimum k_{pol} of $0.1\ cm^{-1}$. However, since measurements of core turbulence[27,28] show maxima around $k_{pol} \sim 1\ cm^{-1}$ (with $k_{pol}\ \rho_S \sim 0.3$), it is important to extend the measurements to lower k in the future.

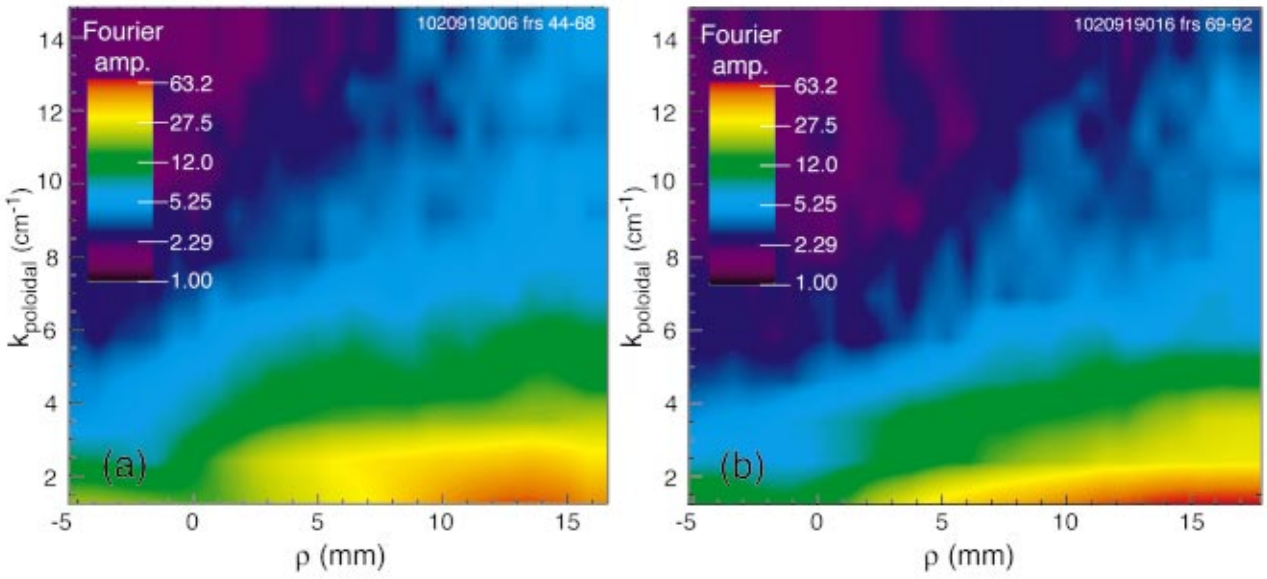

FIG. 5. (Color) Experimental k_{pol} spectra vs ρ for the "high" field case (a) and the "low" field case (b). The color scale (for Fourier amplitude) is as shown.

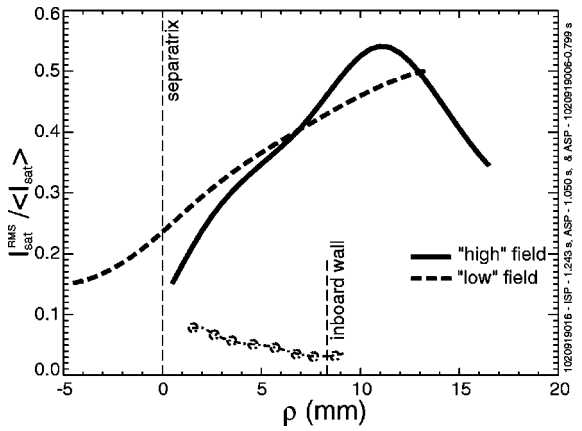

FIG. 6. Normalized I_{sat} fluctuations for the two cases discussed, as measured by the outboard reciprocating probe, and the inboard fluctuation level as measured by another probe scanning through the inboard SOL (open circles). The inboard fluctuation level is measured for the ''low'' field case and is discussed in Sec. V. Similar ratios between inboard and outboard fluctuation levels are seen in the ''high'' field case as well.

Some of the parameters and characteristics of these two discharges are summarized in Table I. Overall, although the SOL density profiles and perpendicular fluxes are quite different, the differences in the turbulence characteristics ($L_{\rm pol}$, $\tau^{\rm exp}_{\rm autocorr}$, and normalized fluctuation level) are not large. As noted, the absolute fluctuation level is different. The details of another experimental $k_{\rm pol}$ spectrum from C-Mod are compared with turbulence simulations in the next section.

IV. COMPARISONS WITH SIMULATIONS AND WITH NSTX OBSERVATIONS

Recent advances in the numerical modeling turbulence now allow detailed comparison with the experimental observations. In particular, we are able to compare directly the characteristics of the 2D (radial and poloidal) turbulence calculated from 3D nonlinear drift-ballooning codes[29–33] with those of the experimental images. A simulation was done using a Non-Linear-Electromagnetic-Turbulence code (NLET)[30] in which time-averaged profiles were specified to be those measured in the outboard SOL of C-Mod. The simulation solves the Braginskii fluid equations for electrons and ions in a 3D geometry (note $\lambda_{ei}/L_c<0.1$). It includes diamagnetic, magnetic shear, and toroidal curvature effects, and, in the limiter shadow region, mimics the effect of open field lines ending on outboard limiters, the nearest of which is 1 m away. A separatrix and X-pt are not included. The inclusion of open lines ending at the divertor does not influence the results and implies that, in regions not in the limiter shadow, the SOL turbulence is not driven primarily by flute-like instabilities in these highly collisional plasmas. Inclusion of open field lines ending on the outboard limiters does alter the shape of the simulation's k spectrum, indicating its importance in setting boundary conditions in the simulation. The global discharge conditions used in the simulation are similar to those of the ''high'' field case discussed above ($B_T=5.4$ T, $I_p=1.0$ MA and $n_e/n_{\rm GW}=0.23$), but from a different shot with different turbulence images.[22] The dominant linear instability leading to the fully developed turbulence in the simulation is the resistive ballooning instability.

A number of quantities calculated in the simulation are compared directly with the experiment, e.g., the simulation and experimental the time-averaged particle fluxes agree to within about a factor of 2. However, a more rigorous test is to compare the $k_{\rm pol}$ spectral shapes vs ρ, as is done in Fig. 7. The simulation's k-spectra are those expected for D_α light emission fluctuations (normalized to the time average), taking into account the expected variation of D_α emission with n_e and T_e,[25] and the simulation's fluctuating density and temperature fields. Thus both parts of Fig. 7 are comparing the same quantity, k-spectra of ''normalized'' emission fluctuations. Also included in the simulation are the effects of a 2 μs time average, and most importantly the measured spatial response of the experimental optical system ($\Delta k_{\rm HWHM}\sim 12\ {\rm cm}^{-1}$). The inclusion of the finite optical response results in the apparent suppression of the smaller-scale features that exist in the simulation's density fluctuation spectrum between $k=5$ and 30 cm^{-1}. The end result is a relatively

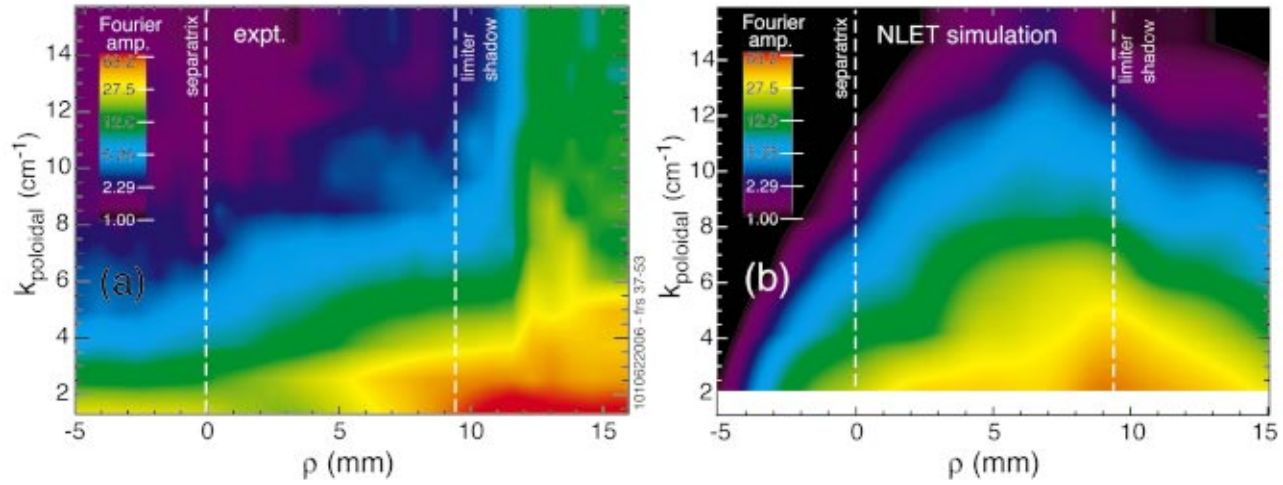

FIG. 7. (Color) Comparison of $k_{\rm pol}$ spectra vs ρ from the experiment (a) with that of the NLET simulation (b). The simulation spectra are post-processed for normalized D_α emission and have the experimental spatial and time resolutions folded in.

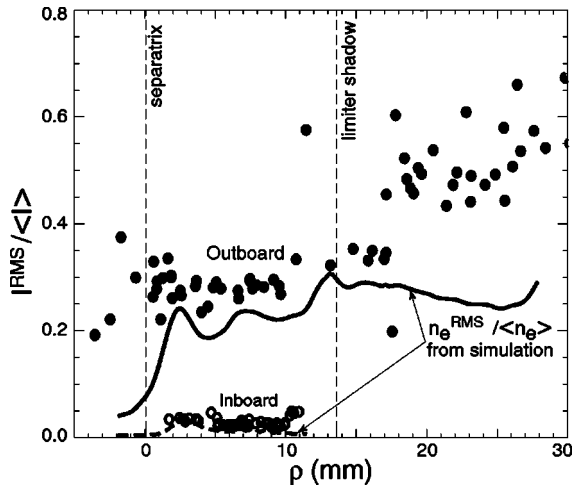

FIG. 8. Normalized intensity (HeI-667 nm) fluctuations, $I^{\mathrm{RMS}}/\langle I\rangle$, as measured by a radially resolving array of tangential views spanning the inboard SOL are compared with those from a radially resolving array of tangential views spanning the outboard SOL. Inboard and outboard probe measurements of $I_{\mathrm{sat}}^{\mathrm{RMS}}/\langle I_{\mathrm{sat}}\rangle$ give similar results, as seen in Fig. 4. (Outboard points are solid circles and inboard are open circles.) Also shown for qualitative comparison are the normalized density fluctuations calculated by an NLET simulation (outboard as solid line and inboard as dashed line).

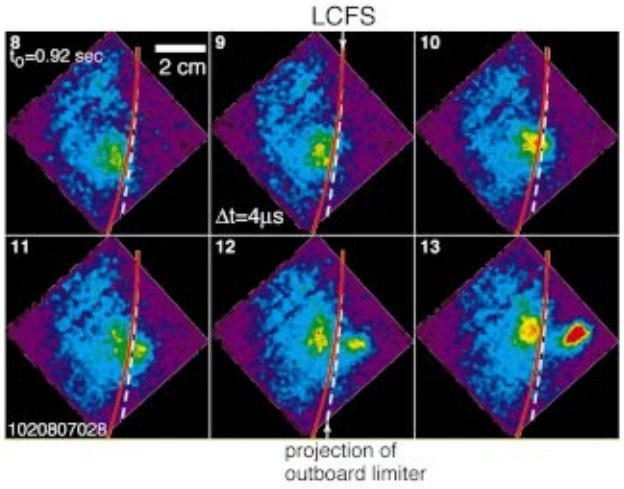

FIG. 10. (Color) Sequences of six experimental images taken at a 250 kHz frame rate, showing space and time evolution of a blob originating inside the LCFS at the outboard SOL. The red line is the LCFS; the black–white line is the toroidal projection of the outboard limiter. The images are emission of the 667 nm HeI line after He has been puffed at the outboard nozzle.

good match between experiment and simulation, shown in Fig. 7. [The minimum nonzero k_{pol} ($\sim 2\ \mathrm{cm}^{-1}$) in the NLET simulation is determined by the 3 cm poloidal extent of the computational grid.] The trends in magnitude and spectral shape are similar for ρ less than about 9 mm. However, there is clear disagreement in amplitude in the limiter shadow, where the simulation shows the relative fluctuation amplitudes decreasing with ρ, while the experiment has the opposite trend. Comparisons of the poloidal turbulence scale length, L_{pol} vs ρ show a good match (within the experimental error of $\sim \pm 25\%$) with the experiment for ρ from 0 to 15 mm. An additional optical diagnostic that measures time histories of the outboard gas-puff emission with D_α filtered, fast diodes[21] from a radial array of views has been used to determine the autocorrelation times characteristic of the fluctuating emission. When comparing these autocorrelation times with the simulation, it is found that the simulation's relatively constant autocorrelation times vs ρ that are a factor of 2 smaller than the measurement inside of $\rho \approx 5$ mm, where $\tau_{\mathrm{autocorr}}^{\mathrm{exp}} \approx 10\ \mu$s, and a factor of ~ 8 smaller at $\rho \approx 10$ mm, where $\tau_{\mathrm{autocorr}}^{\mathrm{exp}} \approx 30\ \mu$s.

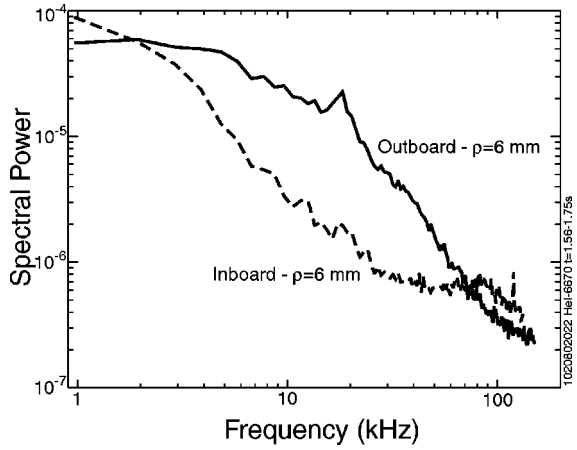

FIG. 9. Comparison of the frequency spectra of intensity fluctuations observed in the inboard (dashed) and outboard (solid) SOLs. The spectra are measured at the same time and are from emission on the same flux surface ($\rho = 6$ mm). The spectra are normalized at ~ 2 kHz.

Thus the match between experiment and NLET simulation is generally good in the region between separatrix and limiter. With the exception of the autocorrelation times (which are strongly affected by plasma flows), the agreement in the quantities compared, time-averaged particle flux, k_{pol} spectrum, L_{pol}, is within a factor of 2. We therefore tentatively conclude that the resistive ballooning instability is providing the turbulence drive, as indicated by the simulation. The simulation appears to include the relevant physics (within the limiter radius), although further comparisons under varying conditions are necessary in order to validate all aspects of the simulation. We note as well that the match is significantly better than the one described in Ref. 22, where an NLET simulation was also compared with similar image data. There are a number of reasons for this. The present case simulated the full SOL profile. It employed the "synthetic diagnostic" technique to calculate the same quantities measured in the experiment (e.g., emission), and it included the local limiters.

An initial comparison with these observations has also been done using another 3D nonlocal electromagnetic turbulence simulation code, BOUT (for boundary turbulence),[31–33] which models boundary-plasma turbulence with a realistic separatrix and X-pt geometry. It also shows a good match with the experimental k-spectrum at a single radial location, although the time-averaged input profiles were somewhat different from those measured. The dominant linear instability is the resistive X-pt mode, which is resistive ballooning in the proper X-pt geometry.

Thus the modeling says that the resistive ballooning mode is the dominant linear instability leading to the devel-

oped, nonlinear, turbulent state in the C-Mod edge. This conclusion was also reached in Ref. 34, where nonlinear simulations showed that resistive ballooning dominates under conditions satisfied in the C-Mod edge, although it should be pointed out that the analysis was in a closed flux-tube geometry. In contrast, it was concluded, based on the analyses of turbulence k-spectra, that the flute-interchange instability with sheath resistivity was responsible for the turbulence observed in the clean SOL plasmas of TEXTOR.[19] This conclusion was also reached in Ref. 18. According to Ref. 19, a simple measure for when the flute-interchange instability dominates is when $(m_e/m_i)^{1/2}(L_c/\lambda_{ei}) \ll 1$, a condition not strongly satisfied in C-Mod (~ 0.4). Hence the high collisionality in C-Mod might be a reason for the difference in the conclusions. It is therefore worthwhile, as an initial step, to see if trends in the characteristic resistive ballooning scale size, L_0, are reflected in the observed turbulence size scales in very different SOL plasmas. A SOL comparison for three specific L-mode discharges is shown in Table I, two are from C-Mod, the ''high'' and ''low'' field cases analyzed above, and the third is from an NSTX L-mode discharge. A number of other experimental quantities are listed in order to point out the differences and similarities in the plasmas and the turbulence characteristics. [L_p^{perp} is the pressure scale length; $L_0 = 2\pi qR[\nu_{ei}\ \rho_S/(2R\omega_{ce})]^{0.5}\ (2R/L_p)^{0.25}$ is the characteristic perpendicular size scale for the (linear) resistive ballooning mode;[28] $L_{\text{pol}}^{\text{turb}}$ is the measured poloidal correlation length of the turbulence; τ_{autocor} is the FWHM of the fluctuation autocorrelation function at a stationary point.]

As seen in Table I, the measured poloidal correlation lengths, $L_{\text{pol}}^{\text{turb}}$, scale only qualitatively with the resistive ballooning mode scale length, L_0. $L_{\text{pol}}^{\text{turb}}$ is from 1.2–4 times larger than L_0. The comparisons also show a rough correlation of $L_{\text{pol}}^{\text{turb}}$ with ρ_S, which would suggest a scaling like $k_{\text{perp}}\rho_S \sim$ constant, although, as noted in the preceding section, the uncertainties are still too large to confirm or deny such a scaling. Thus we conclude that, while the scaling of $L_{\text{pol}}^{\text{turb}}$ is at best qualitatively consistent with the scaling of L_0, such a simple comparison based on linear instability analysis is not sufficient to reveal the turbulence drive, and the full nonlinear simulation is probably necessary.

V. INBOARD/OUTBOARD FLUCTUATION COMPARISONS

The inboard/outboard levels of edge turbulence have also been investigated in C-Mod using both additional inboard-viewing optical diagnostics and an additional inboard fast-scanning Langmuir probe. A second array of tangentially viewing fiberoptics, which image to a *radial* array of 3 mm diameter spots that span the *inboard* SOL just in front of an inboard midplane gas puff, is used to compare normalized intensity fluctuations with those measured by the similar array on the outboard side. Both measure the same emission line from the puffed gas (D_α for D_2 or HeI-667 nm for He) in lower single null discharges. As seen in Fig. 8, the normalized fluctuation level is approximately a factor of 10 smaller than that measured simultaneously *on the same flux surface* at the outboard midplane. The inboard and outboard probe measurements of $I_{\text{sat}}^{\text{RMS}}/I_{\text{sat}}$ yield results similar to those from the optical diagnostics, as can be seen in Fig. 6. (The *absolute* rms level of I_{sat} fluctuations is also significantly higher on the outboard side.) Also shown in Fig. 8 are the inboard/outboard profiles of normalized density fluctuations calculated from the simulation of the plasma discussed in Sec. IV. It is meant for qualitative comparison only, since the time-averaged inboard profiles were not used in the simulation's calculation of the inboard turbulence. (Instead, the outboard profiles for a similar shot were mapped along the flux tube to the inboard side.) Nonetheless, the fractional decrease in the normalized fluctuation level is the same order of magnitude as that measured. Thus the inboard measurements are consistent with the ballooning drive indicated by the simulations.

There are also significant differences in the measured frequency spectra of the inboard/outboard fluctuations. Shown in Fig. 9 are the frequency spectra from the gas-puff emission, one from a view of an outboard puff at $\rho = 6$ mm, the other from an inboard view of a simultaneous inboard puff also with $\rho = 6$. The inboard spectra are clearly much narrower, as seen after arbitrarily normalizing them at 2 kHz.

The literature reveals very little regarding inboard/outboard turbulence comparisons. Reference 1 found coherent fluctuations on the inboard side on ASDEX only when the field lines there connected to the outboard, unfavorable-curvature side (as is the case in the single null C-Mod discharges reported on here). The relative level of inboard/outboard fluctuations was not discussed. Coherent inboard fluctuations were absent in ASDEX double null cases. Also Ref. 35 reports clear observations of filaments on the inboard side of TFTR. Reference 36 measured a significant decrease in radial particle flux on the inboard side for L-mode plasmas in CCT, but found little difference in normalized density and potential fluctuations.

There is another important implication from the C-Mod observation of a low inboard-to-outboard fluctuation ratio. Since the measurements are compared on the same open flux surface, it is unlikely that the SOL turbulence in the C-Mod is driven primarily by flute-like instabilities. In fact any model in which the entire flux tube fluctuates more or less at once is at odds with this inboard/outboard experimental result.

VI. OBSERVATIONS OF BLOBS NEAR THE DENSITY LIMIT

In most C-Mod and NSTX discharges the identifiable blobs are seen *outside* the LCFS. Reference 16 has also noted that they appear to be formed near the LCFS in DIII-D. This has led to speculation that the separatrix and/or open field lines are involved in their generation and/or transport. On the other hand, Refs. 7 and 8 have argued that open field lines are not essential to blob creation, and hypothesize moreover that it is the encroachment of the rapid, intermittent perpendicular transport into the *closed* flux surfaces that leads to the robust Greenwald density limit observed in to-

kamaks. Using gas-puff imaging in discharges near the density limit ($n/n_{GW}=0.7$), we were able to observe ~ 1 cm sized structures—blobs—that were clearly inside the LCFS (Fig. 10). Six frames of a 250 kHz movie are shown in Fig. 10. The red line shows the location of the LCFS, in this case determined by an outboard limiter whose projection is shown by the white–black dashed line. The parameters for this discharge were $I_p=0.61$ MA, $n_e=2.8\times 10^{20}$ m^{-3}, $B_t=5.4$ T. Thus we speculate that the blob generation occurs in the high gradient region, which is typically at the LCFS, but which is observed to move into the closed flux surfaces near the density limit. The generation of localized regions of high vorticity in steep gradient regions is also supported by the simulations.

VII. SUMMARY

The spatial and temporal characteristics of the turbulence in the outboard and inboard SOL of Alcator C-Mod have been investigated using ''gas-puff-imaging'' and probes. With the imaging we identify intermittently occurring structures—blobs—as the phenomenon seen as large amplitude, non-Gaussian-distributed events on probes. The spatial characteristics of the outboard SOL turbulence were determined for two discharge conditions with different field strengths and densities (normalized to the Greenwald density), both different by more than a factor of 2. Poloidal correlation lengths were found to be somewhat different, both in magnitude and radial profile, although the differences are within the measurement uncertainties. Normalized fluctuation levels were similar. The results were compared quantitatively with 3D nonlinear simulations of the C-Mod edge for which the time-averaged profiles were fixed. The agreement between the simulations and the experimental measurements was good for the radial profiles of poloidal correlation lengths. Good agreement was also found in the poloidal wave number spectra over the part of the profile, with significant differences existing in the limiter shadow. The simulations identify the resistive ballooning instability as the dominant linear instability. Inclusion of results measured from the outboard SOL of NSTX allowed comparison of turbulence characteristics over an even greater parameter range in B_T, λ_{ei}/L_c, ρ_s, gradient scale length. There is a rough, but inconclusive, scaling of the turbulence scale size with the resistive ballooning mode scale size. The ballooning character of the turbulence is more clearly evidenced by the experimental comparison between the fluctuation levels in the inboard and outboard SOLs. Both the gas-puff-imaging diagnostics and inboard and outboard fast-scanning probes show normalized fluctuation levels on the inboard side that are typically 5–10 times lower than on the outboard side of the same flux surface. The frequency spectra are also quite different. These observations clearly support a ballooning-like drive and do not support flute-like instability drive for which field line connection to a surface is important. Finally, in discharges close to the density limit, we observe blobs inside the LCFS, implying that their origin is tied to regions of steep gradients, rather than to the boundary between open and closed flux surfaces.

ACKNOWLEDGMENTS

The authors wish to thank Dr. B. Lipschultz, Dr. S. Krasheninnikov, Dr. A. Pigarov, Dr. J. Boedo, and Dr. D. Whyte for helpful discussions.

Work supported by USDOE Cooperative Agreement DE-FC02-99ER54512 (MIT), Contracts Nos. DE-AC02-76CHO3073 (PPPL) and W-7405-ENG-48 (LLNL).

[1] M. Endler, H. Niedermeyer, L. Giannone, E. Kolzhauer, A. Rudyj, G. Theimer, and N. Tsois, Nucl. Fusion **35**, 1307 (1995).
[2] B. K. Joseph, R. Jha, P. K. Kaw, S. K. Mattoo, C. V. S. Rao, and Y. C. Saxena, Phys. Plasmas **4**, 4292 (1997).
[3] R. A. Moyer, J. W. Cuthbertson, T. E. Evans, G. D. Porter, and J. G. Watkins, J. Nucl. Mater. **241–243**, 633 (1997).
[4] Y. Sarazin and Ph. Ghendrih, Phys. Plasmas **5**, 4214 (1998).
[5] M. Umansky, S. I. Krasheninnikov, B. LaBombard, and J. L. Terry, Phys. Plasmas **5**, 3373 (1998).
[6] B. LaBombard, R. L. Boivin, M. Greenwald, J. Hughes, B. Lipschultz, D. Mossessian, C. S. Pitcher, J. L. Terry, and S. J. Zweben, Phys. Plasmas **8**, 2107 (2001).
[7] M. Greenwald, Plasma Phys. Controlled Fusion **44**, R27 (2002).
[8] B. LaBombard, M. Greenwald, R. L. Boivin *et al.*, ''Density limit and cross-field edge transport scaling in Alcator C-Mod.'' Proceedings of the 19th IAEA Fusion Energy Conference, Lyon, France, 2002 (International Atomic Energy Agency, Vienna).
[9] B. A. Carreras, V. E. Lynch, and B. LaBombard, Phys. Plasmas **8**, 3702 (2001).
[10] D. L. Rudakov, J. A. Boedo, R. A. Moyer, S. Krasheninnikov, A. Leonard, M. A. Mahdavi, G. R. McKee, G. D. Porter, P. C. Stangeby, J. G. Watkins, W. P. West, D. G. Whyte, and G. Antar, Plasma Phys. Controlled Fusion **44**, 717 (2002).
[11] S. I. Krasheninnikov, Phys. Lett. A **283**, 368 (2001).
[12] G. Y. Antar, S. I. Krasheninnikov, P. Devynck, R. P. Doerner, E. M. Hollmann, J. A. Boedo, S. C. Luckhardt, and R. W. Conn, Phys. Rev. Lett. **87**, 065001 (2001).
[13] O. Grulke, T. Klinger, M. Endler, and A. Piel, Phys. Plasmas **8**, 5171 (2001).
[14] R. A. Moyer, J. G. Watkins, R. W. Conn, R. Doerner, D. N. Hill, R. Lehmer, R. T. McGrath, L. Schmitz, R. D. Stambaugh, and G. Tynan, J. Nucl. Mater. **196–198**, 854 (1992).
[15] J. A. Boedo, D. Rudakov, R. Moyer *et al.*, Phys. Plasmas **8**, 4826 (2001).
[16] J. A. Boedo, G. McKee, R. Colchin, D. Whyte, D. D'Ippolito, S. Allen, A. Leonard, A. Mahdavi. R. Moyer, M. Schaffer, J. Watkins, and P. West, ''Intermittency and transport in the DIII-D boundary,'' J. Nucl. Mater. (to be published).
[17] S. J. Zweben and R. W. Gould, Nucl. Fusion **23**, 825 (1983).
[18] M. Endler, J. Nucl. Mater. **266–269**, 84 (1999).
[19] A. Huber, A. V. Nedospasov, U. Samm, and B. Schweer, J. Nucl. Mater. **266–269**, 546 (1999).
[20] G. McKee, R. Ashley, R. Durst, R. Fonck, M. Jakubowski, K. Tritz, K. Burrell, C. Greenfield, and J. Robinson, Rev. Sci. Instrum. **70**, 913 (1999).
[21] J. L. Terry, R. Maqueda, C. S. Pitcher, S. J. Zweben, B. LaBombard, E. S. Marmar, A. Y. Pigarov, and G. Wurden, J. Nucl. Mater. **290**, 757 (2001).
[22] S. J. Zweben, D. P. Stotler, J. L. Terry *et al.*, Phys. Plasmas **9**, 1981 (2002).
[23] R. J. Maqueda, D. P. Stotler, J. L. Terry, and S. J. Zweben, Rev. Sci. Instrum. **74**, 2020 (2003).
[24] S. J. Zweben, R. A. Maqueda, J. L. Terry *et al.*, Proceedings of the 29th EPS Conf. On Control. Fusion and Plasma Physics, Montreux, 2002.
[25] D. Stotler, B. LaBombard, J. L. Terry, and S. J. Zweben, ''Neutral transport simulations of gas puff imaging experiments on Alcator C-Mod,'' J. Nucl. Mater. (to be published).
[26] B. LaBombard, M. V. Umansky, R. L. Boivin, J. A. Goetz, J. Hughes, B. Lipschultz, D. Mossessian, C. S. Pitcher, and J. L. Terry, Nucl. Fusion **40**, 2041 (2000).
[27] G. McKee, K. Burrell, R. Fonck, G. Jackson, M. Murakami, G. Staebler, D. Thomas, and P. West, Phys. Rev. Lett. **84**, 1922 (2000).
[28] G. McKee, M. Murakami, J. A. Boedo *et al.*, Phys. Plasmas **7**, 1870 (2000).
[29] B. N. Rogers, J. F. Drake, and A. Zeiler, Phys. Rev. Lett. **81**, 4396 (1998).

[30]K. Hallatschek and A. Zeiler, Phys. Plasmas **7**, 2554 (2000).
[31]X. Q. Xu, R. H. Cohen, G. D. Porter, T. D. Rognlien, D. D. Ryutov, J. R. Myra, D. A. D'Ippolito, R. A. Moyer, and R. J. Groebner, Nucl. Fusion **40**, 731 (2000).
[32]X. Q. Xu, W. M. Nevins, R. H. Cohen, J. R. Myra, and P. B. Snyder, New J. Phys. **4**, 53 (2002).
[33]W. M. Nevins *et al.*, ''Simulations of boundary turbulence in tokamak experiments,'' Proceedings of the 19th IAEA Fusion Energy Conference, Lyon, France, 2002 (International Atomic Energy Agency, Vienna).
[34]A. Zeiler, D. Biskamp, J. F. Drake, and B. N. Rogers, Phys. Plasmas **5**, 2654 (1998).
[35]S. J. Zweben and S. S. Medley, Phys. Fluids B **1**, 2058 (1989).
[36]G. R. Tynan, J. Liberati, P. Pribyl, R. J. Taylor, and B. Wells, Plasma Phys. Controlled Fusion **38**, 1301 (1996).